

ALOS PALSAR OBSERVATION OF KILAUEA VOLCANO ACTIVITIES FROM 2006 TO 2009

Zhe Hu, Linlin Ge, Xiaojing Li, Kui Zhang, Alex Hay-Man NG and Chris Rizos

Cooperative Research Centre for Spatial Information & School of Surveying and Spatial Information Systems,
the University of New South Wales, Sydney, NSW, 2052, Australia
z.hu@unsw.edu.au

KEY WORDS: DInSAR, Ground Deformation, Disaster Mitigation, Kilauea Volcano, Volcano Modelling.

ABSTRACT:

Volcanic eruptions are one of the most serious of nature's calamities, threatening both human lives and property in its immediate vicinity. The dangerous environment surrounding a volcano also causes great difficulties for close-up monitoring and surveillance. A satellite remote sensing technique - Differential Interferometric Synthetic Aperture Radar (DInSAR) - therefore is preferred. In this paper DInSAR is used to survey the deformation of the Kilauea Volcano in Hawaii. A 2D deformation map of Kilauea Volcano, for the period from 26th May 2006 to 3rd March 2009, covering the whole volcanic area, is presented. The minimum time interval of the deformation map is 46 days, which is the repeat cycle of the Japanese ALOS (Advanced Land Observing Satellite) satellite. To address this temporal sampling problem a Simple Volcano-Oriented Deformation Model (SVODM) is proposed, derived from the deformation map, illustrating the changes in the shape of the Kilauea Volcano in the past as well as predicting its future deformation.

1 INTRODUCTION

The Kilauea Volcano (Latitude: $19^{\circ}25'16''N$, Longitude: $155^{\circ}17'13''W$) located on Hawaii's main island is one of the most active volcanoes in the world. It has erupted several times in recent history and became active again on 8th January 2009. Currently the volcano is under close surveillance, with many ground monitoring stations deployed around it (U.S. Geological Survey, 2009). However, these stations are still unable to monitor the whole volcano area, especially the high risk regions. To address this problem the DInSAR remote sensing technique is applied in order to measure the deformation of the Kilauea Volcano.

Compared with traditional ground surveying methods, the satellite DInSAR technique has many advantages for mapping the co-, post- and inter-eruption deformation of a volcano. It is able to survey the volcano remotely, avoiding the need for dangerous close-in study, while centimetre level accuracy and large scale coverage can still be guaranteed. Meanwhile, recent developments in relation to synthetic aperture radar (SAR) satellites make it possible to obtain sufficient data for long term monitoring. Some projects are reported in (Fernandez J. and V., 2002) (Beauducel F. and J-L., 2000) and (Lagios E. and V., 2005), in which the feasibility of using DInSAR for volcano monitoring have been validated.

In the DInSAR method a raw interferogram image is first obtained in order to estimate the ground deformation patterns. The result is obtained by calculating the phase (travel time) difference of radar echoes between the SAR satellite's two passes over the same area, separated by multiples of the satellite repeat period. Then, the topographic phase contribution to the raw interferogram is removed, with the residual phase (differential interferogram) mostly attributable to ground deformation. After a few subsequent processes, such as phase unwrapping (C.W and H.A., 2002), the spatial deformation between two SAR image acquisitions can be finally obtained from the differential interferogram.

ALOS PALSAR (Phased Array type L-band Synthetic Aperture Radar) data/images are used to derive the DInSAR results presented in this paper. The ALOS (Advanced Land Observing Satellite) was launched by the Japan Aerospace Exploration Agency

(JAXA), and is a follow-on satellite mission to the JERS-1 (Japanese Earth Resources Satellite) and ADEOS (Advanced Earth Observing Satellite) missions. The PALSAR sensor carried onboard the ALOS is an L-band SAR imager that can provide about ten metre ground resolution when operated in the Fine Beam Single FBS mode (the range resolution is twenty metres for the Fine Beam Dual FBD mode). It takes 46 days for the satellite to revisit the same site, so the minimum time interval between deformation events is 46 days.

As DInSAR observation can only provide a discrete surveying result over 46 days due to the satellite repeat cycle, a growth model is necessary to describe the continuous deformation state of the monitored volcano. In (Cong X. and A., 2008), a DInSAR-based geophysical stress model was introduced to describe the volcano's deformation. However, such a model is usually assumed to be linear, which could result in some model error for the deformation interpretation. Another model, referred to as the GFM (Geophysical Forward Model), is proposed in (Crippa B. and G., 2008), but it requires as input both ground survey data and DInSAR results, or even information on ground feature. The AEM (Active Elastic Model) is described in (Papademetris X. and J.S., 2001), and now is widely used for modelling and evaluation of seismic deformations. This model reduces the bias in deformation estimation. In this paper a Simple Volcano-Oriented Deformation Model, specifically developed for the Kilauea Volcano, is proposed by combining the deformation statistic results with the simplified AEM model. As a result, detailed and continuous changes of the surface of the Kilauea Volcano can be presented in the deformation map.

2 GENERATION OF THE DEFORMATION MAP

2.1 Description of Target Areas and ALOS PALSAR Data Sets

Kilauea Volcano is located in the southeast part of Hawaii Island, and has two active craters (shown in Figure 1, marked as Crater A and Crater B). All the ALOS PALSAR images used in this study are focused on these two sites. The whole SAR image area is about $30 \times 20 \text{ km}^2$.

In order to obtain a long term monitoring result for the Kilauea Volcano, ALOS PALSAR images taken on Track 287, Frame 38, ascending orbit with 21.5 degrees look angle were selected, with acquisition dates from 26th May 2006 to 3rd March 2009. Other information about these SAR data is listed in Table 1.

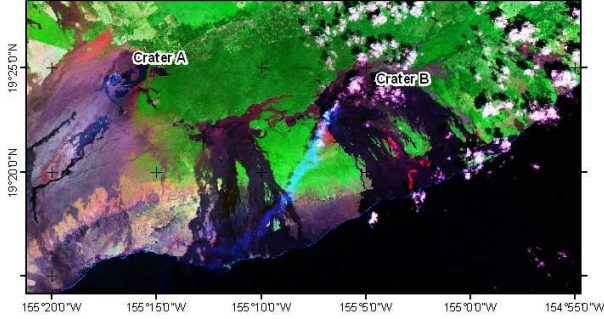


Figure 1: Ground Features of the Kilauea Volcano Area (this satellite image is taken by Landsat 7©).

Acquisition Date	Image Mode
26/05/2006	FBS
11/07/2006	FBS
11/01/2007	FBD
26/02/2007	FBD
14/10/2007	FBS
29/11/2007	FBS
14/01/2008	FBD
29/02/2008	FBD
16/10/2008	FBS
01/12/2008	FBS
16/01/2009	FBD
03/03/2009	FBD

Table 1: Information on ALOS PALSAR Data.

To generate the results, the two-pass DInSAR method (Ge L. and C., 2008)(Ge L. and C., 2007) was adopted in this study. In this approach, two different images in an interferometric pair are needed to calculate one interferogram. Hence 66 interferogram pairs can be obtained through the images listed in Table 1. In fact, in order to illustrate the deformation from the first acquisition date (26/05/2006) and to reduce the intermediate processes, only eleven interferogram pairs are required to cover the whole time span. Considering perpendicular baselines, time coverage and master image status of the interferometric pairs, eleven higher quality pairs have been selected for the deformation map generation. Their details are listed in Table 2.

2.2 Processing Flow of DInSAR Method

For the two-pass method there will be several phase components in the raw interferogram generated by the two different SAR images. Let ϕ_{raw} denote the phase of raw interferogram, then:

$$\phi_{raw} = \phi_{def} + \phi_{topo} + \phi_{prop} + \phi_{noise} \quad (1)$$

where ϕ_{def} is the phase corresponding to the ground deformation, ϕ_{topo} is the topographic phase contribution, ϕ_{prop} is a possible phase delay due to the impact of ionosphere and atmosphere, and ϕ_{noise} is the noise. In DInSAR, all phases except ϕ_{def} should be removed in order to obtain the signal of ground deformation. Normally, ϕ_{def} and ϕ_{topo} are far larger than ϕ_{prop} and ϕ_{noise} , so an approximate value of ϕ_{def} can be obtained

Perpendicular Baseline (metre)	Temporal Baseline (day)	Master	Slave
1441	46	26/05/2006	11/07/2006
351	230	26/05/2006	11/01/2007
2492	276	26/05/2006	26/02/2007
931	230	26/02/2007	14/10/2007
740	276	26/02/2007	29/11/2007
1156	332	26/02/2007	14/01/2008
1545	368	26/02/2007	29/02/2008
1059	598	26/02/2007	16/10/2008
1024	644	26/02/2007	01/12/2008
624	690	26/02/2007	16/01/2009
682	736	26/02/2007	03/03/2009

Table 2: Information on Interferometric Pairs.

when only ϕ_{topo} is removed. The processing flow for DInSAR interferogram generation is illustrated in Figure 2.

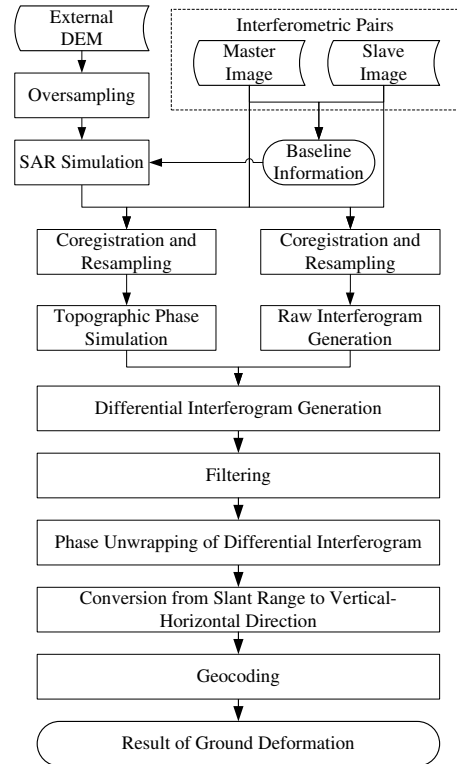


Figure 2: Processing Flow of Two-pass DInSAR.

After the slave image is coregistered to the master image, the phase difference (Raw Interferogram) between them can be calculated using conjugated multiplication. An external DEM (Digital Elevation Model) is introduced so as to compute the topographic phase. Since 90m resolution SRTM (Shuttle Radar Topography Mission) DEM is used in this study, it must be oversampled to correspond to the 10m or 20m resolution of the PALSAR images. Based on the oversampled DEM and baseline information of the master and slave, a simulated SAR image can be generated. Then topographic phase can be obtained, and the differential interferogram can be obtained by removing the topographic phase from raw interferogram. The phase unwrapping step calculates the absolute deformation in the satellite's line of sight (LOS) direction, based on the differential interferogram. The unwrapped result should then be converted to Vertical-Horizontal direction (HVD) so that the vertical ground deformation can be extracted.

2.3 DInSAR Results of the Deformation Map

The geocoded differential interferograms of all eleven pairs are presented in Figure 3. It can be clearly seen that Crater A is deforming during the whole observation period, and Crater B starts to change after 11th January 2007. For these images, with master image acquired on 26/05/2006, the longitude range is from -155.419220° to -154.933006° and latitude range is 19.193439° to 19.512195° . Coverage for images with master image acquired on 26/02/2007 is from longitude -155.398333° to -154.910503° and latitude 19.182409° to 19.501973° .

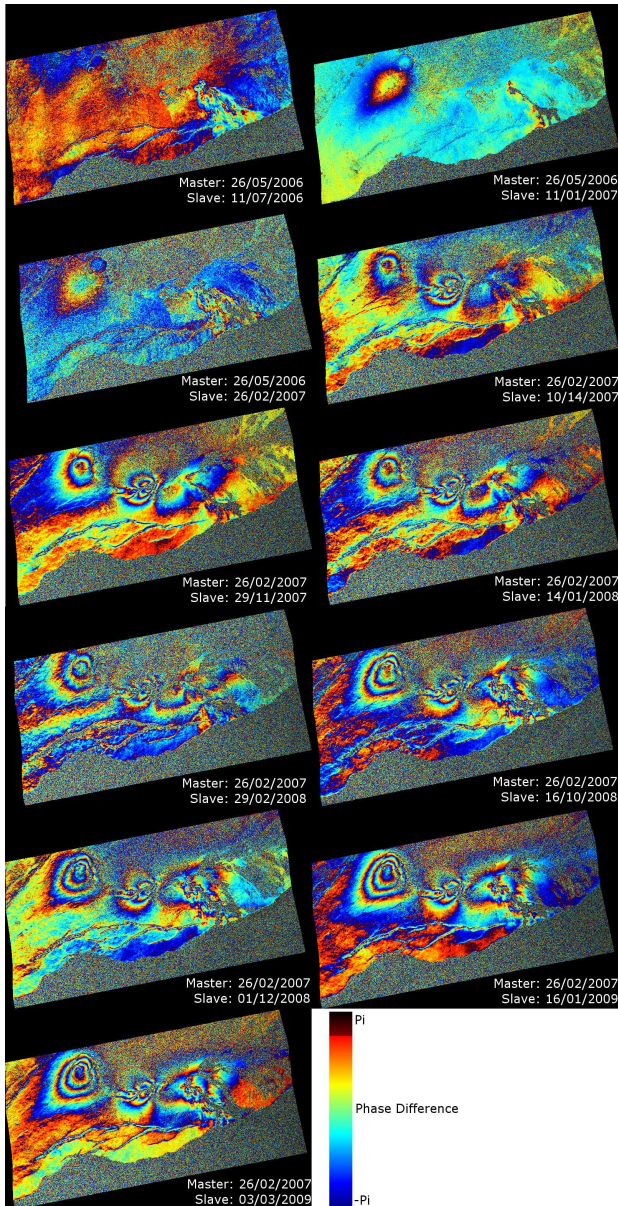


Figure 3: Geocoded Differential Interferogram of Kilauea Volcano.

Phase Unwrapping, followed by geocoding and coordinate transform from LOS to HVD, results in the absolute deformation phase shown in Figure 4. The 2D deformation map can be obtained based on the images with unwrapped phase after a few calculations, such as unit conversion (phase to metre) and deformation accumulation (let all deformations start from 26th May 2006).

To illustrate the movement trends of the Kilauea Volcano more

clearly, Point A and Point B located in the centre of Crater A and Crater B respectively are selected from the phase-unwrapped results to highlight their vertical deformation. The accumulated deformation from 26th May 2006 is shown in Figure 5. It can be clearly seen that the volcano started to subside after 11th January 2007. This phenomenon followed immediately after a major eruption of the Kilauea Volcano in January 2007.

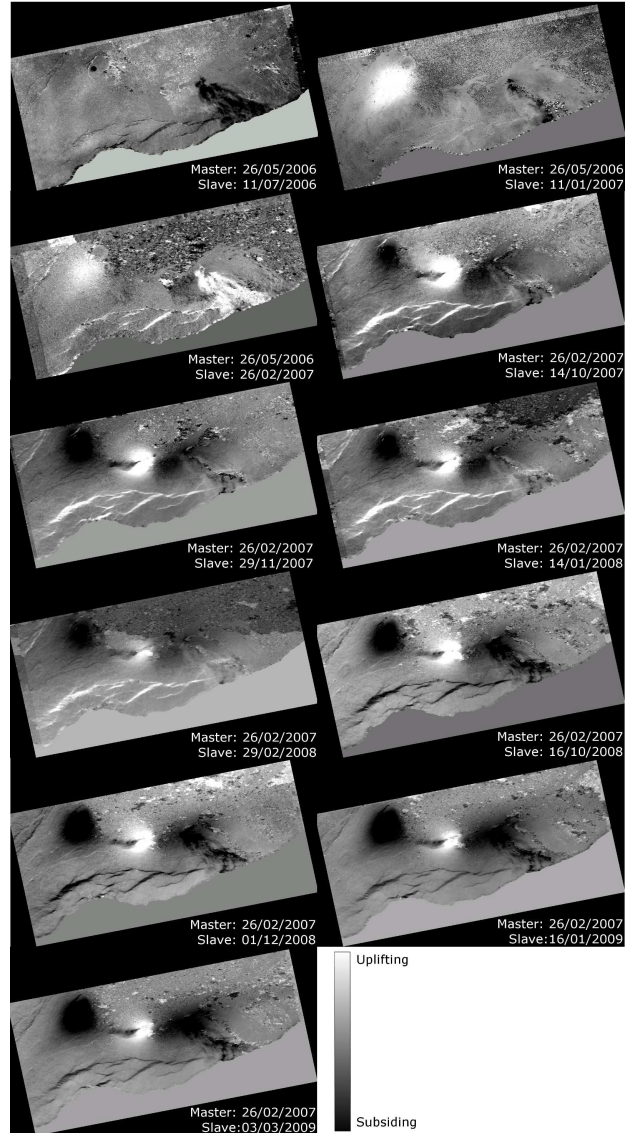


Figure 4: Absolute Phase in Vertical-Horizontal Direction.

3 MODELLING OF THE VOLCANO MOVEMENT

3.1 Mathematical Description of SVODM

The AEM is a widely used model for seismic deformation modelling which assumes that the ground surface is elastic and has quadratic response to the energy. The parameters of the AEM are mainly composed of the elastic properties of materials and energy attributes. As elastic assumption is similar when considering volcano activities, and the material (lava) and the energy source (magma chamber) can be assumed to be uniform, the Simple Volcano-Oriented Deformation Model (SVODM) is obtained as a simplification of the AEM. The principle is illustrated in Figure 6.

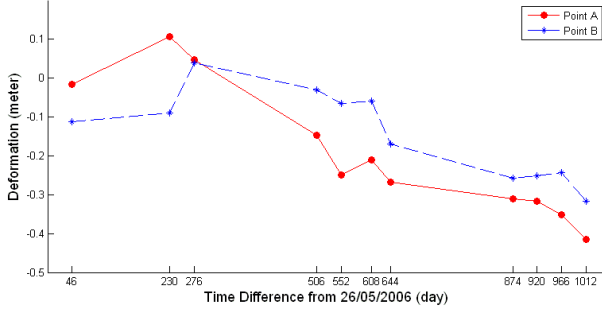


Figure 5: Accumulated Vertical Movement of Point A and Point B.

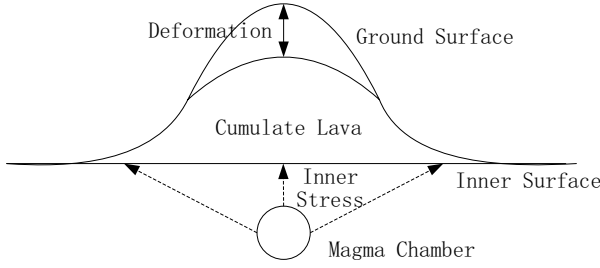


Figure 6: Simple Volcano-Oriented Deformation Model.

According to Figure 6, there are three layers in the SVODM: Ground Surface, Cumulate Lava and Inner Surface. Loads are applied to the Inner Surface by Inner Stress generated by the Magma Chamber, and Inner Stress is in inverse proportion to the distance between points on the Inner Surface and Magma Chamber. As the lava penetrates through the Inner Surface into the Cumulate Lava layer, it is assumed that the Inner Surface remains flat in the SVODM. The forces on the Inner Surface are passed to the Ground Surface by the Cumulate Lava layer to make Ground Surface move. Its squared vertical deformation value is in direct proportion to the Inner Stress in the vertical direction - due to the elastic assumption. The thickness of the Cumulate Lava layer depends on the distance to the projection of the Magma Chamber onto the horizontal plane. According to general principles of statistics, the distribution of layer thickness follows a normal distribution (Gaussian distribution). The weight of the Cumulate Lava layer and the volume of the Magma Chamber are ignored here.

As described above, the vertical force F is:

$$F = \frac{\alpha(t-t_0)}{\sqrt{\frac{(x-x_{mag})^2 + (y-y_{mag})^2 + z_{mag}^2}{|z_{mag}|}}}} \quad (2)$$

$$= \frac{|z_{mag}|^{1/2} \alpha(t-t_0)}{[(x-x_{mag})^2 + (y-y_{mag})^2 + z_{mag}^2]^{3/2}}$$

where (x, y, z) and $(x_{mag}, y_{mag}, z_{mag})$ are Cartesian coordinates of a point on the Inner Surface and Magma Chamber respectively. The position of the Inner Surface is $z = 0$. $\alpha(t-t_0)$ denotes the force coefficient of the Inner Stress, which is a function of the growth time $t-t_0$ of the volcano. t_0 is the first observation time (acquisition time of master image), and $\alpha(t-t_0) = 0$ when $t = t_0$. Since the relationship between the deformation value of the Ground Surface d_{gs} and vertical force F is $d_{gs}^2 = \beta F$ (β is the deformation coefficient of the Ground Surface), the d_{gs} will

be:

$$d_{gs} = \frac{\beta |z_{mag}|^{1/4} \alpha(t-t_0)}{[(x-x_{mag})^2 + (y-y_{mag})^2 + z_{mag}^2]^{3/4}} \quad (3)$$

As a result, the expression for the SVODM is obtained by adding the deformation of the Ground Surface d_{gs} to the thickness of Accumulate Lava h_{al} :

$$SVODM(x, y, t) = d_{gs} + h_{al}$$

$$= \frac{\beta |z_{mag}|^{1/4} \alpha(t-t_0)}{[(x-x_{mag})^2 + (y-y_{mag})^2 + z_{mag}^2]^{3/4}} + \frac{\varepsilon}{\gamma \sqrt{2\pi}} \exp\left[-\frac{(x-x_{mag})^2 + (y-y_{mag})^2}{2\gamma^2}\right] \quad (4)$$

where γ is the lava distribution coefficient, and ε is the thickness coefficient. In equation 4, the only time-related coefficient $\alpha(t-t_0)$ can be estimated from a set of observed deformation values (in this study they are all the unwrapped DInSAR results in the Vertical-Horizontal direction) using the least squares algorithm.

A demonstration of the results of the SVODM is given in Figure 7, with the following parameters: $\alpha(t-t_0) = 10$, $\beta = 1$, $\gamma = 20$, $\varepsilon = 3$, and $(x_{mag}, y_{mag}, z_{mag}) = (0, 0, -20)$. It indicates the deformation between t and the first observation time t_0 .

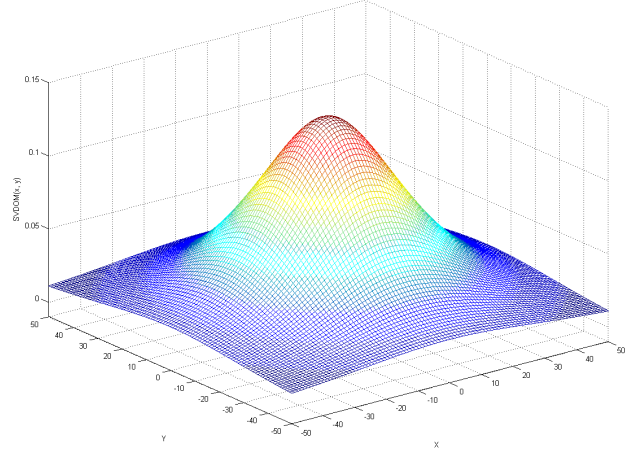


Figure 7: Demonstration of SVODM Result.

3.2 Comparison between Modelling Results and DInSAR Results

The proposed SVODM was fit to the DInSAR observation results, while also considering the SRTM DEM information, and the coefficients of the SVODM for Crater A and Crater B were computed. As a result, the form of the SVODM is given by:

$$SVODM = SVODM_{CA} + SVODM_{CB}$$

$$= \frac{-1.40 \times 10^{-13} \Delta t^4 + 3.25 \times 10^{-10} \Delta t^3 - 2.50 \times 10^{-7} \Delta t^2 + 6.06 \times 10^{-5} \Delta t - 0.047}{[(x+155.277133)^2 + (y-19.403801)^2 + 0.0016]^{3/4}} + \frac{7.81 \times 10^{-15} \Delta t^4 - 8.65 \times 10^{-12} \Delta t^3 - 6.01 \times 10^{-9} \Delta t^2 + 5.85 \times 10^{-6} \Delta t - 0.0089}{[(x+155.145833)^2 + (y-19.375925)^2 + 0.0016]^{3/4}} + 0.05 \cdot \exp\left[-\frac{(x+155.277133)^2 + (y-19.403801)^2}{0.08}\right] + 0.01 \cdot \exp\left[-\frac{(x+155.145833)^2 + (y-19.375925)^2}{0.005}\right] \quad (5)$$

where Δt denotes the time difference between the master image and the slave image acquisitions.

A DInSAR simulation is implemented after equation 5 is obtained, with real satellite imaging parameters. To demonstrate the function of this model, five simulated results for the period 26th February 2007 to 29th November, 2007 (with 69 days interval) are shown in Figure 8. The simulation uses the same master image, acquired on 26th May 2006. The simulated accumulated deformations of Point A and Point B are presented in Figure 9.

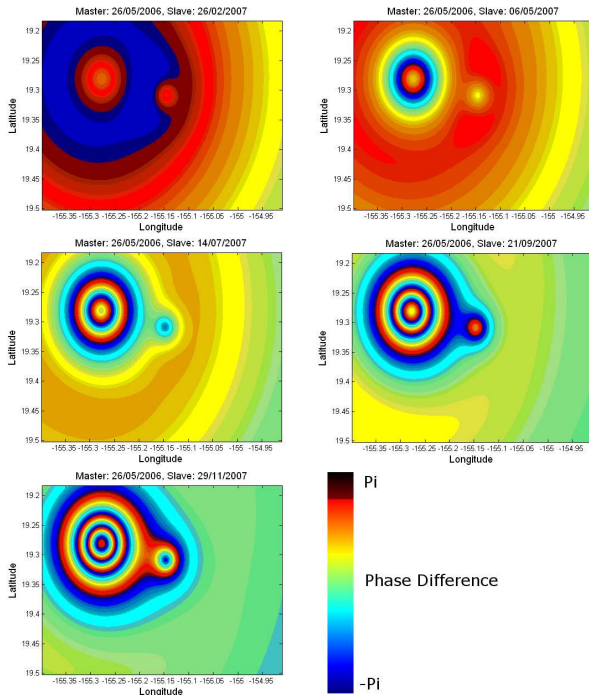


Figure 8: DInSAR Simulation Results based on SVODM.

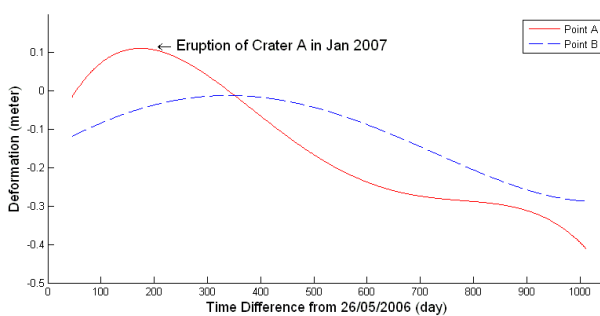


Figure 9: Simulated Accumulated Deformation of Point A and Point B.

Comparing Figures 8 and 9 with the results in Figures 3 and 5 respectively, the SVODM of the Kilauea Volcano fits the DInSAR observation results. According to the GPS monitoring data provided by (U.S. Geological Survey, 2009), there are about 0.3 metres subsidence in the period August 2007 to April 2009. During this period the result calculated from the SVODM is similar. Moreover, by adopting the SVODM the theoretical 2D deformations of the Kilauea Volcano at any time are able to be calculated, which can be used to compensate for missing results during observation time gaps.

4 CONCLUSIONS AND FUTURE WORK

In this paper the DInSAR remote sensing technique has been demonstrated for volcano deformation monitoring. A 2D deformation map was developed based on the surveying results that cover a long time span. The map illustrates the detailed surface changes to the Kilauea Volcano during the observation period. In order to fill in the time gap when no satellite observations were available, the SVODM model was used to represent the continuous deformation of the Kilauea Volcano. From the model results, Crater A grows rapidly when it approaches its eruption time (January 2007). This trend can be used in the prediction of future eruptions. Also, the volcano started to subside after the eruption and no other uplift has been observed till now.

Improvements can generate improved DInSAR results. First of all, only ALOS PALSAR images acquired in the ascending orbit with only one Track and Frame are used here. Images from the descending orbit or other Tracks covering this area should also be used. GPS or other ground surveying result would also be helpful in improving the interferogram (Ge L. and M., 2004). With these strategies, not only more comprehensive observation can be made, but also the time gaps will be reduced. Secondly, the conversion from LOS to HVD is carried out by simply projecting the LOS results to the HVD. With the help of images from the descending orbit, a better conversion method can be used. As to the improvement of the SVODM, the limitation is that only a few coefficients are introduced into this model. Furthermore, the calculation of coefficients of the SVODM used in this study is simply based on the features of the DInSAR images, rather than considering other properties of volcanoes and the surrounding environment. Hopefully, some ground feature-related parameters can be introduced into the SVODM in order to make it more realistic.

ACKNOWLEDGEMENTS

This research work has been supported by the Cooperative Research Centre for Spatial Information (CRC-SI), whose activities are funded by the Australian Commonwealth's Cooperative Research Centres Programme. The Australian Research Council and the Australian Coal Association Research Program have been funding radar related studies by the team at the University of New South Wales (UNSW) during the last few years.

The authors wish to thank the Earth Remote Sensing Data Analysis Centre (ERSDAC) for providing ALOS PALSAR data. METI and JAXA retain the ownership of the ALOS PALSAR original data. The PALSAR Level-1.1 products were produced and provided to the CRC-SI/UNSW by ERSDAC, Japan.

REFERENCES

- Beauducel F., B. P. and J-L., F., 2000. Volcano Wide Fringes in ERS SAR Interferograms of Etna: Deformation or Tropospheric Effect? *Journal of Geophysical Research* 105(B7), pp. 16391–16402.
- Cong X., Hinz S., E. M. and A., P., 2008. Ground Deformation Measurement with Radar Interferometry in Exupry. In: *Second Workshop on Use of Remote Sensing Techniques for Monitoring Volcanoes and Seismogenic Areas*, Nov., Naples, Italy, pp. 1–4.
- Crippa B., Sabadini R., C. M. B. R. and G., P., 2008. Coupling Geophysical Modelling and Geodesy to Unravel the Physics of Active Faults. In: *Second Workshop on Use of Remote Sensing Techniques for Monitoring Volcanoes and Seismogenic Areas*, Nov., Naples, Italy, pp. 1–5.

C.W, C. and H.A., Z., 2002. Phase Unwrapping for Large SAR Interferograms: Statistical Segmentation and Generalized Network Models. *IEEE Transactions on Geoscience and Remote Sensing* 40(8), pp. 1709–1719.

Fernndez J., Romero R., C. D. L. F. and V., A., 2002. InSAR Volcano and Sseismic Monitoring in Spain. Results for the Period 1992c2000 and Possible Interpretations. *Optics and Lasers in Engineering* 37, pp. 285–297.

Ge L., C. H.-C. and C., R., 2007. Mine Subsidence Monitoring Using Multi-source Satellite SAR Images. *Photogrammetric Engineering and Remote Sensing (PE & RS)* 73(3), pp. 259–266.

Ge L., Li X., R. C. and M., O., 2004. GPS and GIS Assisted Radar Interferometry. *J. of Photogrammetric Engineering and Remote Sensing* 70(10), pp. 1173–1178.

Ge L., Zhang K., N. A. D. Y. C. H.-C. and C., R., 2008. Preliminary Results of Satellite Radar Differential Interferometry for the Co-seismic Deformation of the 12 May 2008 Ms8.0 Wenchuan Earthquake. *Geographic Information Sciences* 14(1), pp. 12–19.

Lagios E., Sakkas V., P. I. and V., D., 2005. Ground Deformation of Nisyros Volcano (Greece) for the Period 1995c2002: Results from DinSAR and DGPS Observation. *Bulletin of Volcanology* 68(2), pp. 201–214.

Papademetris X., Onat E.T., S. A. D. D. C. R. and J.S., D., 2001. The Active Elastic Model. In: *Proceedings of the 17th International Conference on Information Processing in Medical Imaging*, Jun., Davis, CA, USA, pp. 36–49.

U.S. Geological Survey, 2009. "Recent Kilauea Status Reports, Updates, and Information Releases.", <http://volcanoes.usgs.gov/kilaueastatus.php>